ZnO and Au/ZnO thin films: room-temperature chemoresistive properties for gas sensing applications

A. Gaiardo[*,1,4], B. Fabbri[1,3], A. Giberti[1,2], V. Guidi[1,2,3], P. Bellutti[4], C. Malagù[1,3], M. Valt[1], G. Pepponi[4], S. Gherardi[1], G. Zonta[1], A. Martucci[5], M. Sturaro[5], N. Landini[1]

[1] Department of Physics and Earth Science, University of Ferrara, Via Saragat 1/c, 44122 Ferrara, Italy

[2] MIST E-R s.c.r.l., Via P. Gobetti 101, 40129 Bologna, Italy

[3] CNR-INO – Istituto Nazionale di Ottica, Largo Enrico Fermi 6, 50124 Firenze, Italy

[4] MNF - Micro Nano Facility, Bruno Kessler Foundation, Via Sommarive 18, 38123 Trento, Italy

[5] Department of Industrial Engineering - University of Padova, Via Marzolo 9, 35131 Padova, Italy

Abstract

Zinc Oxide has been widely investigated for its photocatalytic properties, which enhance the bulk/surface charge transfer at room temperature. At the same time, the doping of semiconductor materials with metals allows the modification of their physical and chemical properties, and hence their performance as gas sensors. The aim of this work was to investigate the difference between thin-film sensors based on pure ZnO nanoparticles and on gold-cluster decorated ZnO in photo-activation mode. The nanopowders were synthesized through simple sol-gel methods and chemically, morphologically and structurally characterized. Thin films were deposited by spin coating onto alumina substrates. The sensing layers were tested with several gases in photo-activation mode, illuminated with radiation wavelengths of 525, 468, 400 and 385 nanometers. Gold-decorated ZnO thin film showed some interesting features, such as better chemoresistive properties than pure ZnO under photo-activation mode, when illuminated with a wavelength of 385 nm. A selective response of the sensing film to NO_2 under green light irradiation was observed, in particular in dry air condition. Furthermore, the humidity effect on the sensing responses was investigated, highlighting a possible application of Au/ZnO for the detection of few ppm of SO_2 with a high percentage of relative humidity.

Keywords: gas sensors, room temperature, ZnO, gold decorated ZnO, thin films

---

* Corresponding author. Tel. +39 0532 974230
E-mail address: andrea.gaiardo@unife.it

1. Introduction

Nowadays, the demand for fast response, cost effective and portable sensors for toxic/hazardous gases detection is growing, due to their exploitation in protecting human lives as well as in the environment monitoring [1, 2]. Among the chemoresistive sensing materials, Metal Oxides Semiconductors (MOS) are the most used nanostructures in gas sensors manufacturing [3-8]. In the last years, due to the growing interest in highly performing gas sensors, the need of morphological control on metal-oxide nanostructures has been taken into account for the optimization of their synthesis processes and the tunability of their properties. Among the wide assortment of metal-oxide materials, the high correlation between the morphology and the intrinsic properties of ZnO makes it stand out. Indeed, the adopted ways to prepare ZnO nanostructures significantly affect their sensing properties [9]. Therefore, it is possible to control the physical and chemical properties of the obtained product by choosing an appropriate synthesis method [10]. Some progresses have been achieved, either by using ZnO nanostructures [11, 12] or a combination of different materials, e.g., noble metal-ZnO [13, 14] and p–n hetero-contact systems [15-18]. It is well known that, through surface functionalization by noble metals such as Pd, Au, and Pt, the sensing performances of semiconductor layers can be significantly enhanced [19-23]. Among these, Au nanoparticles decoration on ZnO surface has been widely studied with respect to their electronic [24], optical [25] and catalytic properties [26].

As gas sensor, ZnO has shown properties in line with the “3s rule”, exhibiting good sensitivity, selectivity and stability over the time [27]. But it is well known that MOS sensors, despite some attractive features, i.e., high sensitivity, fast and reversible response, reduced dimensions and low cost of manufacturing, metal-oxide films operation show a drawback that is a relatively high energy consumption, occurring during film operation, since the reversibility of surface reactions between the semiconductor nanoparticles and the gaseous molecules occurs at high temperatures (200-600°C) [28]. Among the well-trodden ways studied to overcome this problem, photo-enhanced gas sensing appeared to be a high potential and suitable solution for room temperature operation [29-31]. With this aim, researchers identified a class of semiconductor materials, which exhibit both chemoresistive and photoconductive properties. Actually, the irradiation of the surface with proper wavelengths provides the

material with more active sites for gas-surface reactions, thus avoiding the need of high temperature operations. This is, for example, the case of both tungsten trioxide (WO_3) and zinc oxide (ZnO). For these solutions, light exposure enables gas sensing at room temperature [32-35]. In particular, ZnO is a typical wide-band gap semiconductor, which has been proven to be efficient in various applications such as the realization of gas sensors [36-38], electronic devices [39] and electrodes for DSSCs [40].

In order to develop ZnO gas sensors, capable of working at low temperatures, light illumination can be employed to increase carrier concentration in the semiconductor conduction band and to promote photo-desorption mechanisms. As well known, the adsorbed oxygen atoms on n-type semiconductor surfaces (e.g., ZnO) are negatively charged and a built-in-field is originated. Photons, with higher energy than that of the band-gap, promote the separation of the electron–hole pairs produced. As the built-in-field is a result of the oxygen chemisorption, surface gas adsorption/reaction has a significant effect on surface photoconductivity. In case of decoration of ZnO nanostructures with gold nanoclusters further improvement of the material photoconductivity can be achieved while its catalytic behaviour is also enhanced [41].

So far, the sensing behaviour of gold-decorated ZnO nanostructures have been extensively studied in thermo-activation mode [42], but only few researches have investigated the effect of the radiation on the improvement of chemoresistive properties of Au/ZnO. In particular, these works studied the interaction of Au/ZnO with a restrained number of gaseous molecules, and the photo-activation mechanism was investigated with a specific excitation wavelength, usually the UV [43]. Recently, Gogurla et al. have showed the sensing performance of an Au/ZnO plasmonic device activated with diverse radiation wavelengths and tested with several gases [44].

The present work is paying more attention to both detected molecules and radiation wavelengths aspects. Recently, we reported [45] the investigation about the difference between the chemoresistive properties of thin- and thick-films made of pure nanostructured ZnO in photo-activation mode. This study highlighted better sensing features of thin films with respect to those of thick films. Starting from these results, we decided to focus the attention on the sensing properties of thin layers of pure ZnO and of ZnO decorated with gold clusters nanoparticles. ZnO was synthesized via a simple sol-gel route, whereas Au/ZnO was produced through an innovative, fast and inexpensive method. Afterwards the powders were chemically, structurally and

morphologically characterized. Thin films were spin-coated onto alumina substrates with interdigitated electrodes. The chemoresistive properties of the films were probed vs. different gases (at TLV-STEL concentration) under photo-activation mode by using four LEDs as radiation sources: green (525 nm), blue (468 nm), violet (400 nm), and UV (385 nm) light. The measurements, carried out in dry air, showed interesting results. Gold decorated zinc oxide highlighted a higher selectivity and higher response to several gases than pure ZnO. At the same time, according to the literature [45, 46], obtained results showed for almost all gases a stronger chemoresistive interaction between chemical compounds and semiconductor nanoparticles as the energy of the radiation approached the ZnO band-gap. In these conditions, a greater and faster response and a quicker recovery time of the gas sensors were recorded in comparison to those obtained by using lower energy radiation [47]. Moreover, an interesting effect was observed in presence of NO_2 by illuminating Au/ZnO thin film with sub-energy bandgap radiation. Indeed, under these conditions, the sensors showed a higher selectivity to NO_2 than for the other wavelengths, with a response that was improving as the incident radiation energy was approaching that of the gold plasmon peak. Furthermore, the humidity effect on the chemoresistive properties for both materials was also investigated. The measurements showed a drastic decrease in sensing response of pure ZnO to all gases under test, meanwhile Au/ZnO layer highlighted a possible application to detect few ppm of SO_2 with high percentage of Relative Humidity (%RH).

2. Experimental details

2.1 Synthesis of ZnO powder and film deposition

ZnO powder (named pure ZnO) was synthetized by standard sol-gel technique. The ZnO solution was prepared by dissolving 300 mg of zinc acetate dehydrate in 2 mL of ethanol. Then, monoethanolamine was dropwise added under fast stirring, keeping the ratio between the metal ion and the amine equal to 1. The solution was stirred for 60 min.

ZnO decorated with gold nanoclusters (Au/ZnO) was prepared by a precipitation method using Gold(III) Bromide ($AuBr_3$) as precursor. A molar concentration of 4.2 $mmol \cdot L^{-1}$ $AuBr_3$ solution was heated at 80°C. The pH was adjusted to 7 by dropwise addition of a NaOH solution. Approximately 1 g of ZnO was dispersed in the

solution. This dispersion caused a pH change, so it was re-adjusted to 7 by consequent dropwise addition of an HCl solution. Thus, the suspension was heated at 80°C and stirred for 2 h. The products were washed several times with distilled water to remove Bromide ions residual as well as the unreacted Au species. After washing, calcination is needed to allow the decomposition of gold precursors to their metallic state. This procedure was carried out at 450°C for 4 h.

Obtained powders were mixed with an ethanol solution and thus deposited by spin-coating technique at 2000 rpm for 30 seconds on two substrate types of, a transparent glass for the optical absorption measurements and an alumina substrate with interdigitated electrodes for the electrical measurements. Thin films were thermally stabilized at 100°C for 10 minutes in air atmosphere. The process of spinning/stabilization was repeated up to 4 times. Films thickness, measured by ellipsometry, resulted to be 250 nm. A final annealing at 500°C for 1 hour in air was performed. The alumina substrate was finally bonded on a suitable support to be interfaced with the electronic measuring system.

2.2 Characterizations

Both the powders and the films of pure ZnO and Au/ZnO were analysed through Scanning Electron Microscopy and Energy Dispersive X-Ray spectroscopy (SEM-EDX spectroscopy), in order to investigate the chemical composition and the morphology of the obtained materials. The instrument used was a Zeiss EVO 40 microscope with an acceleration voltage of 30 kV.

The crystalline phase of the films was characterized by X-ray diffraction (XRD), using a Philips PW1710 diffractometer, provided with glancing-incidence X-Ray optics. The analysis was carried out at 0.5° of incidence, employing Cu Kα Ni-filtered radiation at 30 kV and 40 mA.

The optical absorption spectra of the samples were measured in the 300-900 nm range using a Jasco V-570 standard spectrophotometer. Optical sensor functionality was studied by making optical absorbance measurements over the wavelength range 350 nm $< \lambda <$ 800 nm, using a custom-made gas flow cell coupled with a Jasco V-570 standard spectrophotometer. Further details are reported in Ref. [48].

Total reflection X-Ray Fluorescence (TXRF) was exploited for elemental analysis of the sample composition in order to identify possible contamination. Measurements have been performed with a Phoenix (TNX, Italy) theta-theta diffractometer modified (DfP, Italy), to allow the placement and integration into the software of a Silicon Drift Detector (SDD) with an active area of 50 mm² (Ketek, Germany) to acquire photons emitted by the sample. The instrument is equipped with a Mo tube, which was operated at 40 kV and 30 mA and a parabolic graded multilayer monochromator (AXO, Germany) aligned to select the Mo Kα radiation. An aliquot of the sample powder was dispersed on a silicon wafer (a part of a 6" <100> wafer) used as sample support. The sample was irradiated at 0.08°; the SDD was placed at 90° with respect to the 0-incidence angle direction. The measurements were carried out with 200 seconds of real time acquisition (40% dead time) on the Au/ZnO sample, on a ZnO sample and on the Si-substrate, used as a support for the Au/ZnO sample.

2.3 Gas sensing measurements

The thin-film sensing properties were tested in a dedicate gas-flow chamber, at room temperature of 23°C, controlled with a commercial thermometer. The surface layers were illuminated with commercial LEDs, of wavelengths 385, 400, 468 and 525 nm. In order to focus the radiation on the sensing areas, the experimental setup was equipped with an optical lens. The LEDs powder at the sensing surface was measured through a commercial Hamamatsu photodiode. The measured values are reported in Table I. Gases from certified bottles and synthetic air (20% O_2 and 80% N_2) were mixed and fluxed through mass-flow controllers. In order to investigate the sensing behaviour of the nanostructured materials and to highlight the differences between pure ZnO and Au/ZnO layers, several gaseous compounds were tested. The gas concentrations were chosen in according to the Threshold Limit Values (TLV) [49, 50], i.e. CO (10 ppm), methane (2500 ppm), acetaldehyde (10 ppm), acetone (10 ppm), butanol (5 ppm), methanol (5 ppm), NO_2 (5 ppm), and SO_2 (10 ppm). In the case of methanol, we focused on concentrations far below its TLV. For the other compounds, we injected concentrations of the same order of TLV, except for the case of acetone, whose odour threshold is 50 times lower than TLV, therefore we used a half concentration value with respect to odour threshold.

The sensing measures were carried out both in dry air and in wet air, the relative humidity in the test chamber has been controlled with a commercial HIH-4000 Honeywell humidity sensor, and the humidity was injected as reported in [51]. In dry air, the relative humidity measured was below 1%.

Gas responses, defined in the following way:

$$R = \begin{cases} (G_{gas} - G_{air})/G_{air} & for\ reducing\ gases \\ (G_{air} - G_{gas})/G_{gas} & for\ oxidizing\ gases \end{cases} \quad (1)$$

were obtained by measuring the conductance (G) variations of the films as a function of the gases tested.

In case of *n*-type semiconductors, the response to reducing (oxidizing) gases is positive (negative); the opposite holds for *p*-type semiconductors.

3. Results and discussion

3.1 Chemical, morphological and structural characterizations

The results of XRD measurements of the synthesized nanopowders are shown in Fig. 1. All films after annealing at 500°C were crystalline, as confirmed from XRD patterns. Diffraction peaks of wurtzite hexagonal ZnO (ICDD No. 36-1451) and cubic Au (ICDD No. 04-0784) were detected in the samples, according to the relative compositions, confirming that annealing at 450°C is sufficient to promote the oxides crystallization and the Au ions reduction. The Au ions reduction inside sol–gel oxide matrixes has been already investigated by [52]. This phenomenon approximately occurred at 200°C, due to the decomposition of gold chloride species and to the oxidation of organic compounds that can donate electrons, thus reducing noble metal ions [53]. By analysing the ZnO reflections, it is clear that the (002) diffraction peak is much more intense than the predicted value; this fact indicates an extensive orientation along the c-axis. Performing a Lorentzian fit on the XRD peaks and measuring the full width at half maximum (FWHM), the mean crystallite diameter of ZnO was estimated to be 29 nm, by means of the Scherrer's relationship, while for Au it was 20 nm.

Figure 1: X-Ray Diffraction patterns of the powders of pure ZnO and gold nanoclusters decorated ZnO powders.

Figure 1

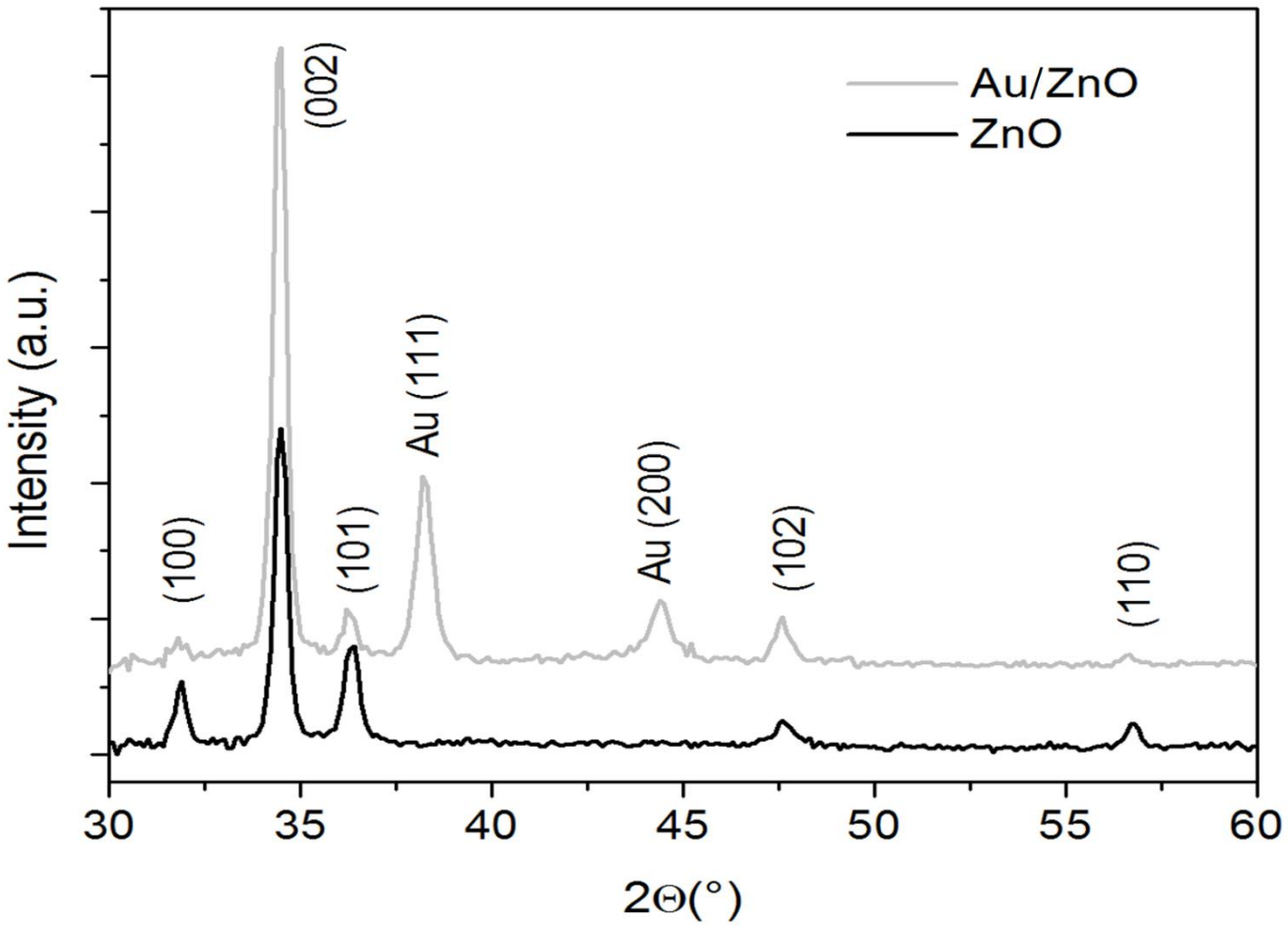

Figure 1: X-Ray Diffraction patterns of the powders of pure ZnO and gold nanoclusters decorated ZnO powders.

The SEM-EDX characterizations are reported in Fig. 2. The SEM images in Fig. 2a and 2b highlighted the nanometric size of the grains, which compose the films. In particular, in Fig 2b, the presence of the Au clusters can be noticed. The EDX chemical analysis showed a high degree of purity for both pure ZnO and Au/ZnO. Moreover, the weight concentration of Au, detected in the layer of Au/ZnO, was about 5.3%.

Figure 2

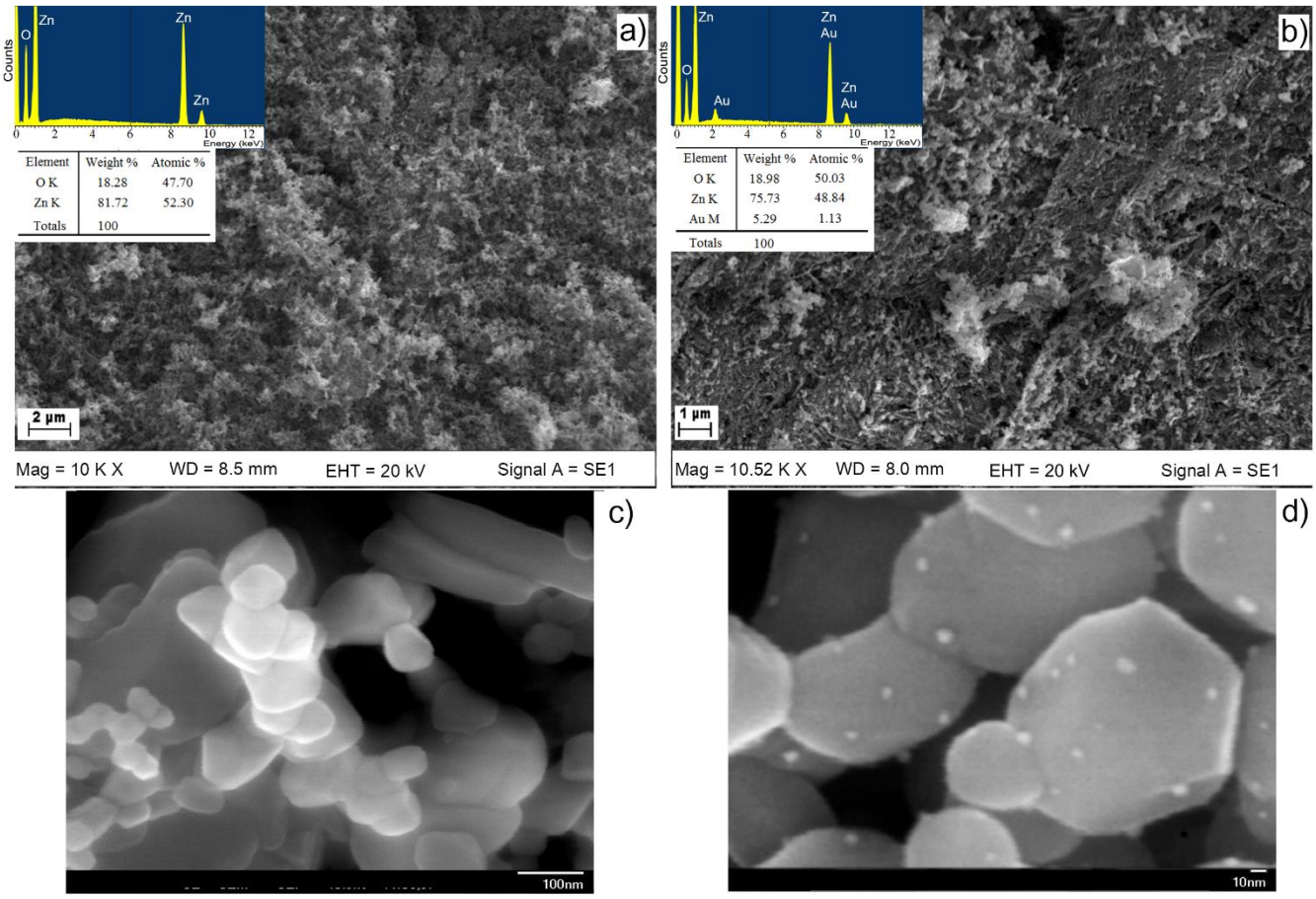

Figure 2: SEM-EDX analysis of *a)* and *c)* pure ZnO, *b)* and *d)* ZnO gold nanoclusters decorated.

Optical absorption spectra of the ZnO and Au/ZnO films, deposited on SiO_2 substrates, are shown in Fig. 3. The absorption spectrum of ZnO film in air follows the typical curve of ZnO, which is transparent in the visible and in near-infrared (NIR) range and presents an absorption onset in the UV, in the range of 350-370 nm, due to the zinc oxide band-gap. In the spectrum of Fig. 3, the exciton peak typical of low dimensional ZnO crystals is also evident [32]. For the Au/ZnO film, the presence of Au NPs is clearly confirmed by the localized surface plasmon resonance (LSPR) peak, recorded at ≈ 590 nm, while outside the LSPR range, the absorption of Au/ZnO sample is overlaid to the pure ZnO film.

Figure 3

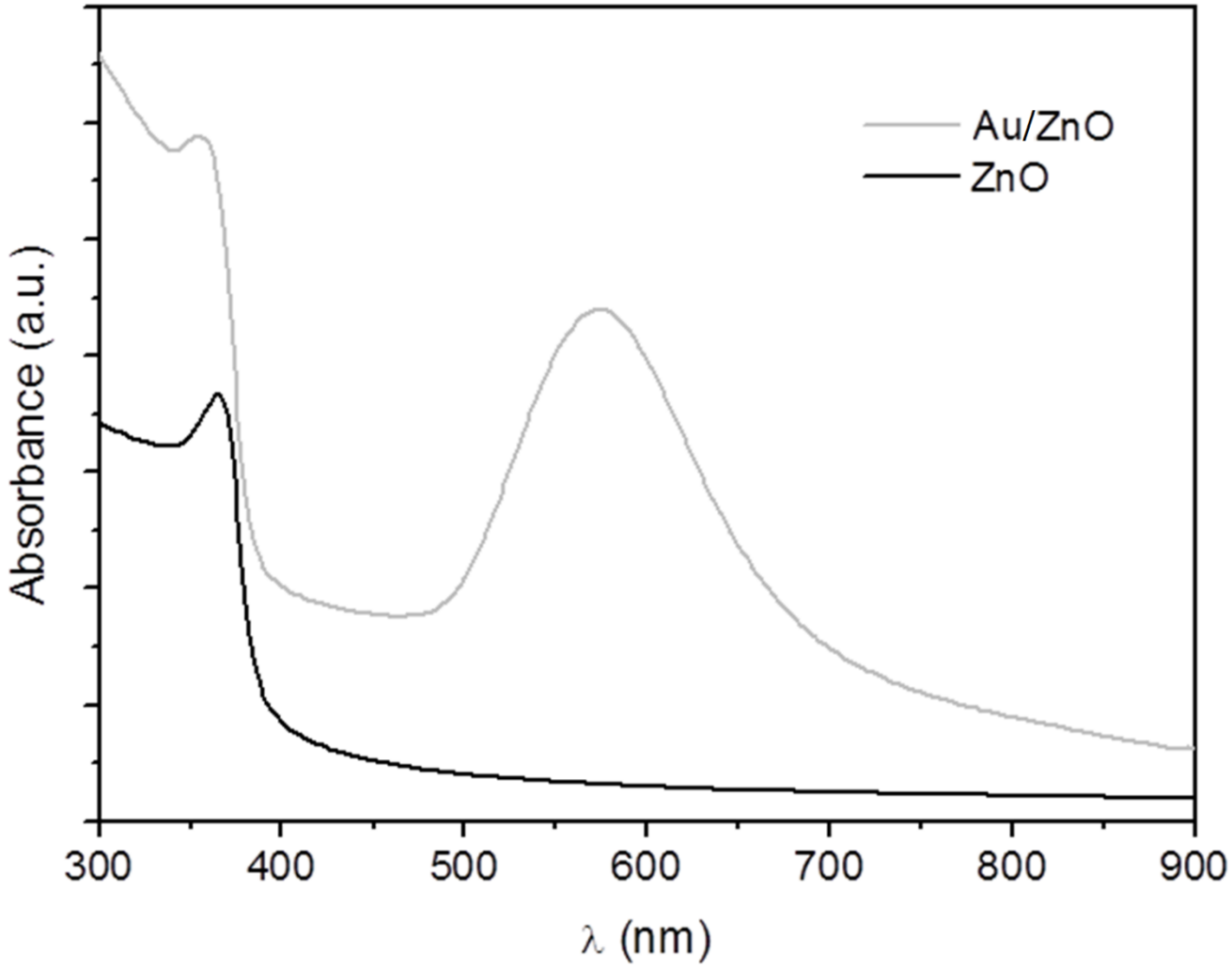

Figure 3: UV-Visible absorption spectroscopy analysis of pure ZnO and ZnO gold nanoclusters decorated.

Fig. 4a shows the Total Reflection X-Ray Fluorescence (TXRF) analysis of pure ZnO and Au/ZnO nanopowders. The quantification was performed by ab initio simulation of the fluorescence spectrum. The Fig. 4b shows experimental and simulated spectra in the region of interest used for the least squares minimization, employed to estimate the Au content with respect to Zn. The estimated atomic gold-to-zinc ratio was of 0.0193 (corresponding to 0.045 weight fraction of Au in a ZnO matrix). In order to fit properly the region containing the Au and Zn peaks, bromine was added to the model sample with a concentration of 0.0014 weight fraction. The spectra in Fig. 4a showed Fe Kα and Ni Kα peaks, mainly due to environmental contamination rather than in

the sample, since they are also visible in the blank wafer spectrum. Analysis highlighted the high purity of the obtained ZnO and detected a very little contamination of bromine in the Au/ZnO sample (0.14 atomic%).

Figure 4

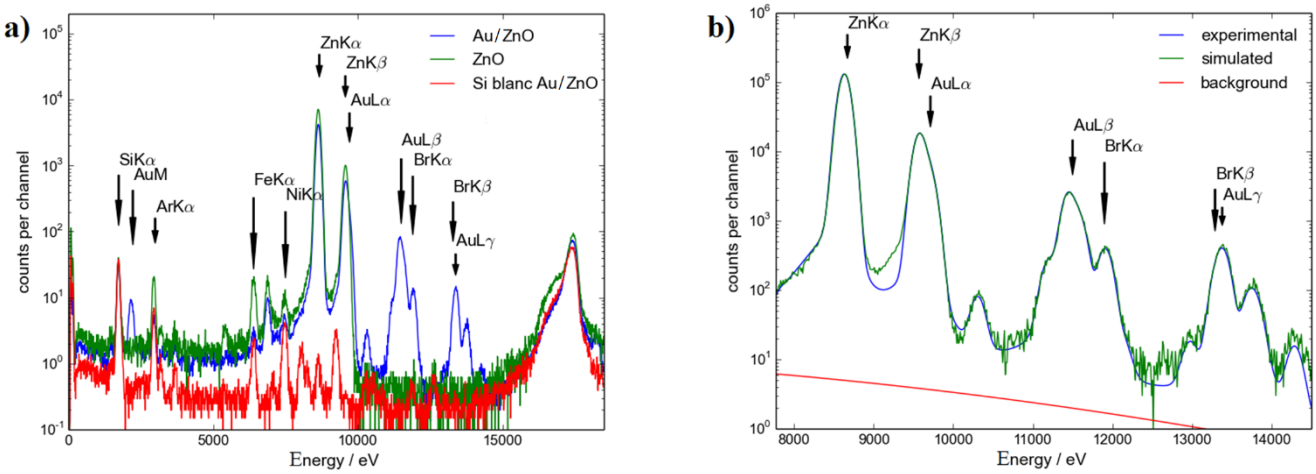

Figure 4: Total Reflection X-Ray Fluorescence (TXRF) analysis of a) pure ZnO and gold nanoclusters decorated ZnO. b) Magnification of the Au/ZnO TXRF.

3.2 Electrical characterizations of the thin films

The aim of this study was to compare the sensing properties of pure ZnO and gold-decorated ZnO thin films, at room temperature under photo-activation mode. The sensors were first stabilized in dry air, under continuous illumination of diverse radiations wavelengths (i.e., 385 nm, 400 nm, 468 nm, 525 nm). For each radiation energy, several gases were tested. We chose to limit the exposure time at 25 minutes since usually, within this time, thin-film sensors tested in photo-activation mode reach the 90% of the maximum response value, by using our experimental setup. Fig. 5 summarizes the responses obtained with the two sensing materials, tested in presence of selected gases in dry air. It can be observed that, for both pure ZnO and Au/ZnO films, the highest responses were obtained with butanol, methanol and sulphur dioxide. At the same time, the conductance variations of the films recorded in presence of CO, acetone, acetaldehyde and methane were negligible. Conversely, the measurements performed with 5 ppm of NO_2 resulted in a significant signal for almost all radiation wavelengths we tested. However, the case of NO_2 deserves deeper considerations, which will be discussed in Section 3.3.

Figure 5

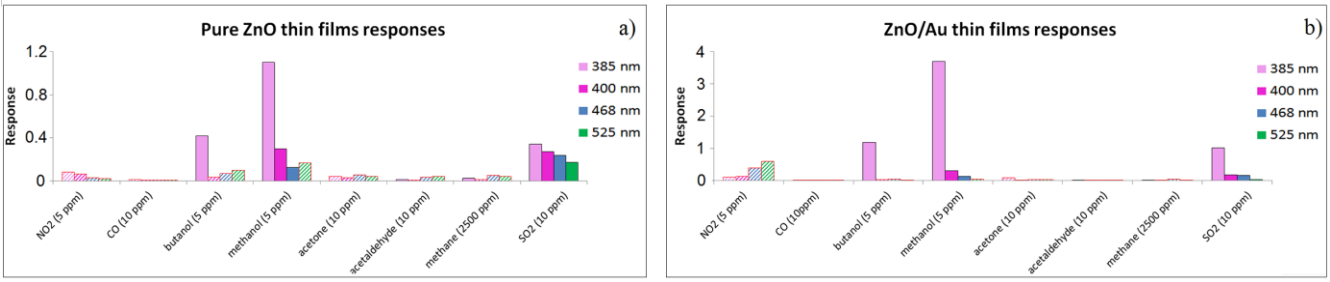

Figure 5: Summary of *a)* pure ZnO and *b)* Au/ZnO thin films responses to all tested gases. The full coloured columns represent reducing responses, whereas the striped columns represent the oxidizing responses.

The above mentioned highest responses, achieved with butanol, methanol and SO_2, were obtained by illuminating both the sensing films with a radiation wavelength of 385 nm. This behaviour has already been observed in previous works [45,46], in which it was demonstrated that a more effective chemoresistive interaction occurs between analytes and ZnO nanoparticles as the energy of the incident radiation approaches the ZnO band gap (3.37 eV). The responses of Au/ZnO films, excited with a radiation wavelength of 385 nm, to butanol, methanol and SO_2, were significantly higher than those obtained with pure ZnO layers, as it can be seen in Fig. 5. With this excitation wavelength, the ratio between the responses of Au/ZnO and pure ZnO films remains constant ($R_{Au/ZnO}/R_{ZnO} \approx 3$) for the three gases. Moreover, it can noticed that the ratio between the responses obtained at 385 nm of radiation and those obtained at different radiation wavelengths was significantly higher in the case of Au/ZnO films (e.g. for methanol $R_{385}/R_{400} \approx 12$) than pure the ZnO ones (e.g. for methanol $R_{385}/R_{400} \approx 3.7$). It is also interesting to highlight that, for butanol and methanol, pure ZnO films showed a different behaviour (oxidizing/reducing) in the interaction between their surface and chemical compounds. This anomalous phenomenon occurs for all the four radiation wavelengths used in the sensors electrical characterization, and it could be ascribed to an induced conductivity switching in ZnO thin film, as reported in literature for nitrogen dioxide [54]. Here, two competing mechanisms were suggested to occur: a change in charge carrier density and a participation of oxygen vacancies.

Fig. 6 shows the dynamic response to 5 ppm of methanol of pure ZnO and Au/ZnO films in dry air. One can observe, for both the films, that a better kinetics of the reaction occurred when the layers were photo-activated

with the wavelength of 385 nm, with respect to the other three wavelengths. This behaviour was also obtained with almost all the other tested gases and could be a consequence of the low-radiation energy, which allows the formation of only few hole-electron pairs. The last could be dragged by the electric field toward the surface, where they would be annihilated by electrons trapped in the surface states, resulting in desorption process and restoration of conductance level. Instead, when the energy of the excitation wavelength is significantly lower than the energy of the semiconductor band-gap, no efficient photo-activation occurs to create a sufficient number of electron-hole pairs. Indeed, in the presence of oxygen, the density of charged surface states (O^-/O_2^-), remains sufficiently high to cause the pinning of Fermi level [55-57], resulting in a great decrease of the semiconductor surface reactivity in presence of few ppm of chemical compounds.

Figure 6

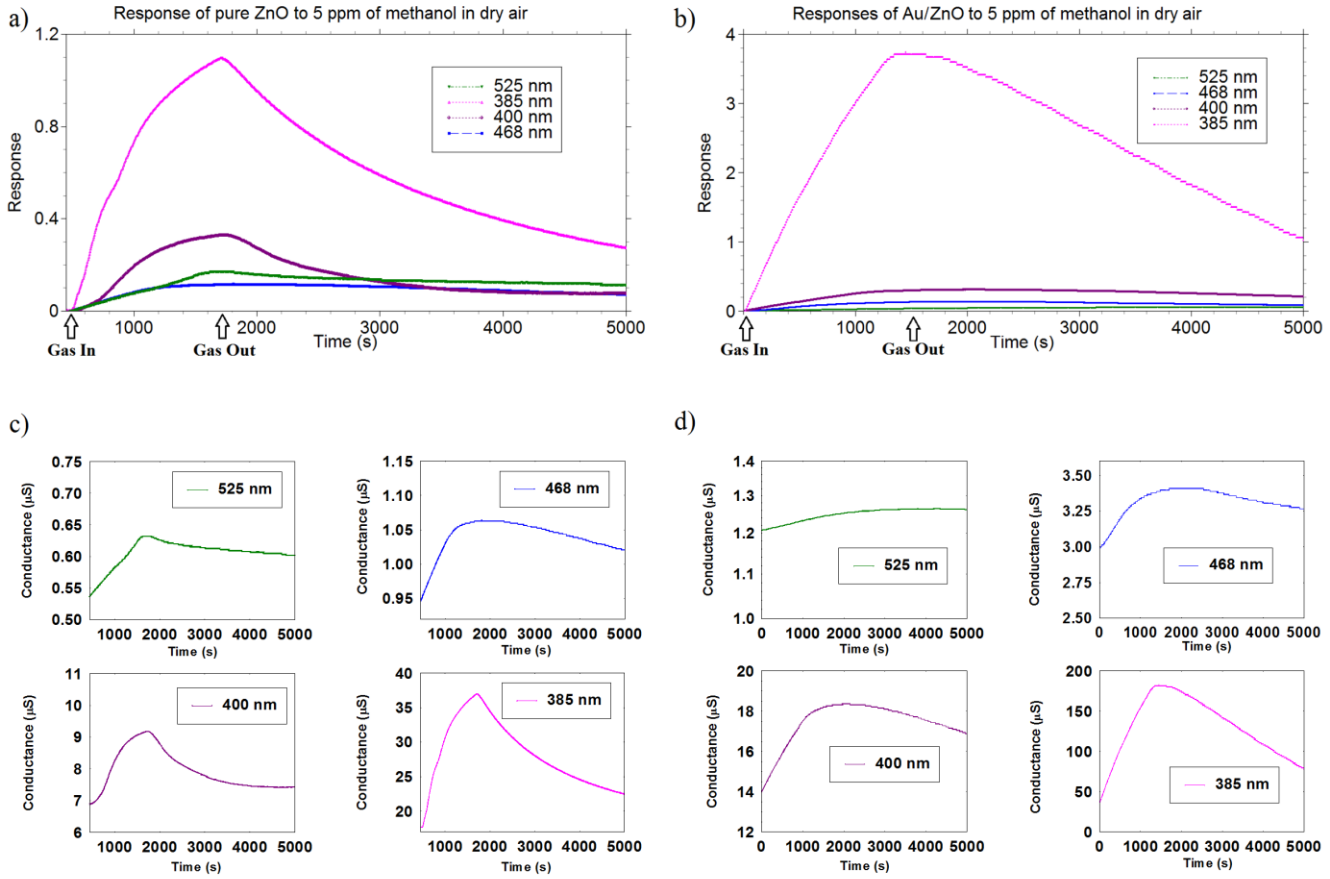

Figure 6: Dynamic responses and conductance transients of *a)* and *c)* pure ZnO, *b)* and *d)* Au/ZnO, to 5 ppm of methanol at 385 nm, 400 nm, 468 nm, 525 nm of excitation wavelengths. The input and output times of methanol are marked on the figure with GAS IN and GAS OUT, respectively.

Moreover, Fig. 6 highlights a faster response and recovery time (calculated as 1/e of the response value) of Au/ZnO than pure ZnO when photo-activated with UV LED (385 nm). This behaviour was also confirmed with the other gases analysed, in particular with SO_2 (Fig. 7) and butanol.

Figure 7

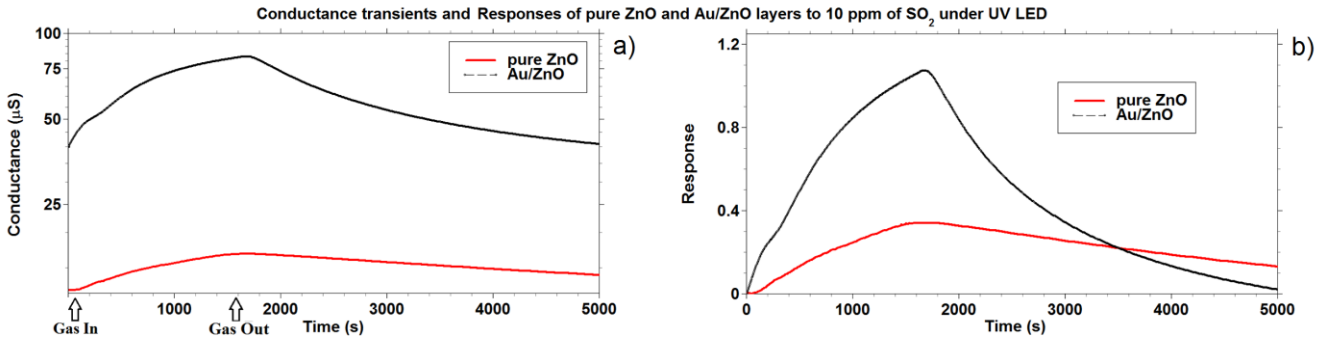

Figure 7: *a)* Conductance transients and *b)* dynamic responses of pure ZnO and Au/ZnO to 10 ppm of SO_2 at 385 nm of excitation wavelength.

The influence of humidity on the gas sensing properties of ZnO and Au/ZnO sensors was also investigated. The characterization was performed for those analytes that gave the better chemoresistive properties in dry air for the ZnO and Au/ZnO layers. We tested butanol, methanol, SO_2 and NO_2 by using the incident radiation wavelength of 385 nm, and NO_2 with the green LED. Gas concentrations were the same used for the sensing characterization in dry air. The measures were carried out with relative humidity of 20%, 40%, 60%, and 80%. The sensing responses to 5 ppm of methanol and butanol decreased drastically already at 20% RH for both materials, vanishing at 40% RH. This trend is probably due to the interaction between the OH^- groups of water with the sensing layers, which hindered interaction of hydroxyl groups contained in the alcohols.

The SO_2 sensing characterization in wet air highlighted interesting features of the sensing layers. The recorded temperatures were 23.2°C (RH% = 20%), 23.1°C (RH% = 40%), 23.4°C (RH% = 60%) and 23.7 (RH% = 80%). Considering pure ZnO, the response to SO_2 quickly decreased when relative humidity was increased. At the same time, the recovery times became much longer than the one in dry air, resulting in incomplete recovery at relative humidity higher than 60%. On the contrary, Au/ZnO sensors showed a gradual response decrease to 5

ppm of SO_2 when humidity was increased, but the response remained significant even at 80% of relative humidity, as shown Fig. 8. Furthermore, the recovery times in wet air were similar to each other as compared to the measurement carried out under dry air. Regarding NO_2, the results obtained will be discussed in the next paragraph.

Figure 8

Conductance transients and Responses of Au/ZnO sensors to 10 ppm of SO_2 in wet air

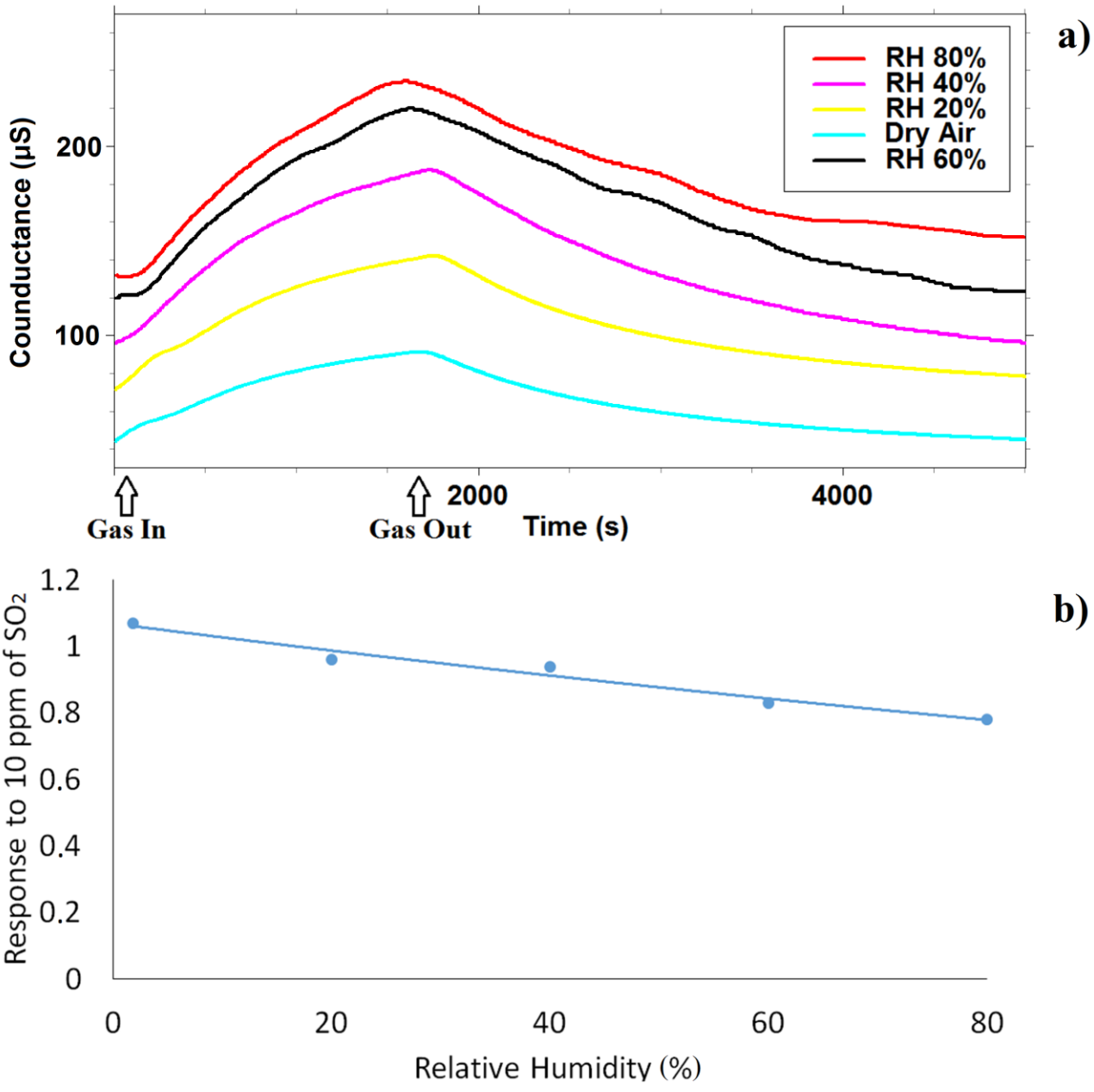

Figure 8: *a)* Dynamic Responses of Au/ZnO to 10 ppm of SO_2, reported as conductance transients, at 385 nm of excitation wavelength, in dry air and in presence of 20%, 40%, 60% and 80% of Relative Humidity; *b)* response values of ZnO/Au to 10 ppm of SO_2 vs. %RH.

The better chemoresistive properties of Au/ZnO than pure ZnO, which arose in Fig. 5 and 6 and 7 especially at 385 nm of excitation wavelengths, were clearly due to the gold nanoclusters and they can be explained by means of two main reasons. First, the limiting factor that controls the efficiency of light-excited single oxide semiconductor photocatalysts is the high-rate recombination of the photo-generated charge carriers [58]. In Au/ZnO layers, the presence of gold nanoclusters leads to an efficient charge separation of the photo-generated electron-hole pairs in Au, which modifies the photocatalysts properties on the ZnO surface and, consequently, increases the lifetime of the photo-generated pairs. This condition allows longer time for the charge carriers diffusion and also for their migration on the catalysts surface, which promote redox processes in the valence and in the conduction bands of the semiconductor [59]. Hence, this enhancement can be explained through an "electronic mechanism" as well as a "chemical mechanism". In the "electronic mechanism", the Au nanoclusters act as electron acceptors on the ZnO surface, contributing to the increase of the depletion layer by a compensation effect [60]. Therefore, with respect to the pure oxide case, the change in the resistance results larger, leading to the increase in response. In the "chemical mechanism", Au catalytically activates the dissociation of molecular oxygen, whose ionic products diffuse to the ZnO nanograins [61].
As far as the second reason, it concerns the high activity, as heterogeneous and homogeneous catalyst, of unsupported Au nanoparticles in the process of oxidation and reduction of several VOC types, as reported in previous works [62, 63].. The role of the catalyst is under continuous discussion and different mechanisms have been proposed [64]. Based on the above considerations, the better chemoresistive properties of Au/ZnO than pure ZnO are addressed.

3.3 The specific case of NO_2

The oxidizing character of NO_2 in the interaction with semiconductor catalysts surface is well known, both under thermo- and photo-activation modes [12, 45]. The responses of ZnO and Au/ZnO films to NO_2, reported in Fig. 5, confirmed this behaviour for all the four radiation wavelengths. The reaction most probably occurring between this chemical compound and the sensing layers of ZnO and Au/ZnO is [12]:

$$NO_2 + e^- \rightarrow NO_2^- \text{ (ads)} \quad (2)$$

The above reaction causes a decrease of electron density at the surface of the semiconductor layer, which undergoes an increase in resistance, this being observed in our sensing measurements. Others type of VOCs, which show this behaviour with activated catalysts, are CO_2 and O_3.

Although the responses in Fig. 5 confirm the better ability of Au/ZnO and ZnO sensors to detect gaseous compound at 385 nm, they show a peculiar characteristic of the two sensing materials in the case of NO_2. NO_2 measurements with pure ZnO sensors show the same trend of the other gases tested, i.e., a higher response as the wavelength radiation approaches the energy of the ZnO band gap, whereas Au/ZnO films highlight the a clear different behaviour. In fact, the latter presented an increase of the response to NO_2 as the energy of the incident radiation decreased, and it showed a major chemoresistive interaction under green-light irradiation (525 nm) with respect to the other three wavelengths tested. This feature is also highlighted in Fig. 9, which shows the dynamic responses of the two sensing films to 5 ppm of nitrogen dioxide as a function of the incident radiation wavelength. The kinetics of the interaction between this chemical compound and pure ZnO layers appears to be slower than that showed by Au/ZnO films, and it is coupled with a lack of reversibility of the former (except for 385 nm), as extensively discussed in Ref. [45]. Instead, for Au/ZnO films, the responses to NO_2 resulted reversible for all radiation wavelengths used.

Figure 9

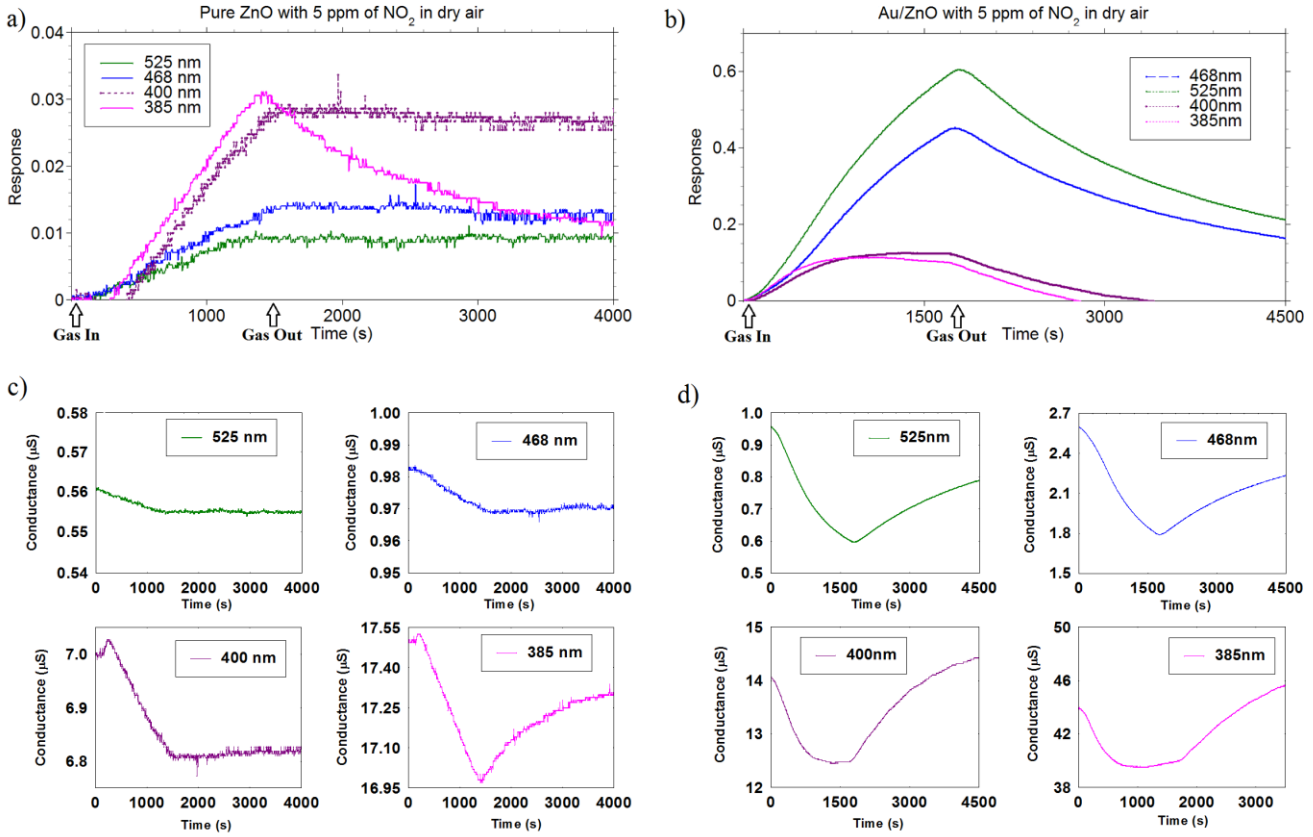

Figure 9: Dynamic responses and conductance transients of *a)* and *c)* pure ZnO, *b)* and *d)* Au/ZnO, to 5 ppm of NO_2 at 385 nm, 400 nm, 468 nm, 525 nm of excitation wavelengths.

As introduced before, the behaviour of Au/ZnO layers with NO_2 is different from both pure ZnO tested with the same gas and from Au/ZnO tested with the other gaseous compounds Au/ZnO. Indeed, with nitrogen dioxide, the reversible and highest response for Au/ZnO sensors was obtained with green light (525 nm), and not at 385 nm as for pure ZnO films. At the same time, the responses achieved for the other chemical compounds tested with Au/ZnO at 525 nm of excitation were negligible. From the sensing point of view, the behaviour of Au/ZnO tested with NO_2 under green light radiation is quite interesting for a possible use of this sensor in the selective detection of nitrogen dioxide at room temperature in dry air. Furthermore, sensing tests carried out in wet air shown that the responses of ZnO and Au/ZnO layers to 5 ppm of NO_2 decrease quickly with 385 nm as incident radiation, and they became negligible at 60% RH. On the contrary, the sensing response of Au/ZnO to NO_2 was still interesting even in wet air, when the layers were photo-activated with the green LED (525 nm). It

is worth noting that the conductance variation of the sensors remained measurable up to 80% RH, although the recovery times became longer compared to the one measured in dry air. The sensing response to NO_2 of Au/ZnO in wet air is reported in the Fig. 10. Testing temperatures in the test chamber were 23.0°C (RH% = 20%), 23.7°C (RH% = 40%), 24.2°C (RH% = 60%) and 23.9°C (RH% = 80%).

Figure 10

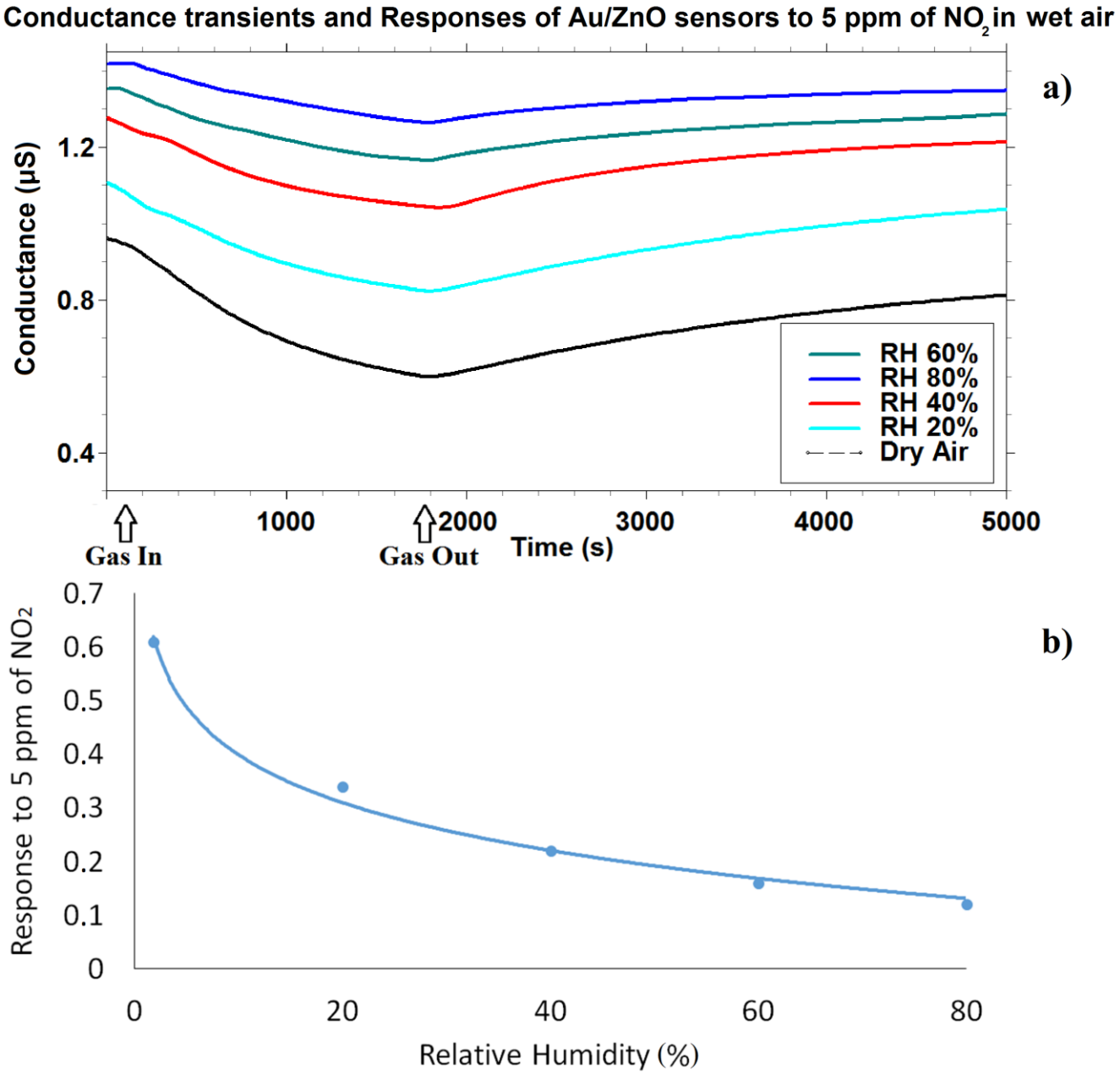

Figure 10: *a)* Dynamic responses of Au/ZnO to 5 ppm of NO_2, reported as conductance transients, at 385 nm of excitation wavelength, in dry air and in presence of 20%, 40%, 60% and 80% of Relative Humidity; *b)* response values of Au /ZnO to 5 ppm of NO_2 vs. %RH.

A possible interpretation of the NO_2 reactivity on Au/ZnO layers under green light could lie in an accentuated photocatalysis property of gold nanoclusters due to its surface plasmon resonance which is near to 525 nm, and this could play a fundamental role. Sarina et al. [65] and Murkherjee et al. [66] demonstrated that when gold nanoparticles are illuminated with a suitable radiation energy, conduction electrons in the 6sp band of gold nanoparticle surface gain energy from absorption of light via the LSPR effect, and then migrate to the higher energy levels of 6sp band through an intraband migration. These "hot electrons", which shift to the higher energy levels, can be captured by oxidizing molecules such as oxygen or, as is our case, NO_2. Then, in the case of the interaction between Au/ZnO films and NO_2, this gold feature leads to a greater change in layers conductance and to an improvement of chemoresistive properties. In order to understand the mechanism that occurs at the surface between the nanostructured material and NO_2, which is out of the scope of this work, it would be necessary to follow the reactions by using a proper technique, such as XANES, and to test other oxidizing gases at different radiation wavelengths.

4. Conclusion

This work presents a comparison between the chemoresistive properties of pure nanostructured ZnO and gold nanoclusters decorated ZnO, at room temperature in photo-activation mode by using LEDs as light source with four incident radiation wavelengths. Eight target gases, belonging to different classes of chemical compounds, were used to carried out the tests (CO, methane, acetaldehyde, acetone, butanol, methanol, NO_2, SO_2).

Both materials, synthesized with simple, fast and inexpensive methods, showed significant responses to butanol, methanol and sulfur dioxide under an incident radiation wavelength of 385 nm in dry air. This behaviour was probably due to an effective chemoresistive interaction between analytes and semiconductor nanoparticles as the

energy of the radiation approaches the ZnO band-gap energy. Indeed, the ZnO photo-enhanced with UV radiation led to better performance of gas sensors, i.e., greater and faster responses but also a quicker recovery time compared to those obtained for the same analytes by using radiations with lower energies.

However, it has been clear observed that Au/ZnO showed better chemoresistive properties than pure ZnO due to the electric and catalytic effects of gold nanoclusters. More precisaly, the sensing responses of Au/ZnO layers were higher and the recovery time was faster with respect to pure ZnO. Furthermore, the measures carried out in wet air highlighted that the sensing responses to butanol and methanol became negligible in case of both MOS undes evaluation, whereas the responses to SO_2 of Au/ZnO sensors remained significant up to 80% of relative humidity.

Moreover, Au/ZnO sensors exhibited an unexpected behaviour with NO_2. Actually, it has been observed that in presence of this gas, the response of the sensing material shows a maximum response at a lower energy with respect to the ZnO band gap. This has been correlated with the activation of plasmon effect since the maximum response was observed by using green light (525 nm) source, which has an energy close to the gold plasmon peak. This result opens up to the possibility to detect selectively NO_2 at room temperature, in particular in dry air.

Acknowledgments

Thanks to Daniela Palmeri of the Ferrara Centre of Microscopy. This work was supported by Programma Operativo FESR 2007-2013, Regione Emilia-Romagna – Attività I.1.1.

References

1. S. Capone, A. Forleo, L. Francioso, R. Rella, P. Siciliano, J. Spadavecchia, et al., Solid state gas sensors: state of the art and future activities, J. Optoelectron. Adv. Mater. 5 (2003) 1335–1348.
2. P. Kim, J. Albarella, J. Carey, M. Placek, A. Sen, A. Wittrig, et al., Towards the development of a portable device for the monitoring of gaseous toxic industrial chemicals based on a chemical sensor array, Sens. Actuators B: Chem. 134 (2008) 307–312.

3. K. Seshan, HANDBOOK OF THIN-FILM DEPOSITION PROCESSES AND TECHNIQUES, 2nd edition, William Andrew publishing, ISBN 0-8155-1442-5.
4. E. Comini, V. Guidi, M. Ferroni, G. Sberveglieri, Detection of landfill gases by chemoresistive sensors based on titanium, molybdenum, tungsten oxides, IEEE Sens. J. 5 (2005) 4–11.
5. G. F. Fine, L. M. Cavanagh, A. Afonja, R. Binions, Metal Oxide Semi-Conductor Gas Sensors in Environmental Monitoring, Sensors 10 (2010) 5469–5502.
6. P. Gouma, Nanostructured oxide-based selective gas sensor arrays for chemical monitoring and medical diagnostics in isolated environments, Habitation 10 (2205) 99-104.
7. T.Z. Fabian, J.L. Borgerson, P.D. Gandhi, C.S. Baxter, C.S. Ross, J.E. Lockey, J.M. Dalton, Characterization of Firefighter Smoke Exposure, Fire Technology 50 (2014) 993-1019.
8. V.S. Vaishnava, S.G. Patelb, J.N. Panchal, Development of ITO thin film sensor for the detection of formaldehyde at room temperature, Sens. Actuators B 202 (2014) 1002-1009.
9. Wang, L., Wang, S., Zhang, H., Wang, Y., Yang, J., Huang, W. Au-functionalized porous ZnO microsheets and their enhanced gas sensing properties, (2014) New Journal of Chemistry, 38 (6), pp. 2530-2537
10. Sahu, D., Panda, N.R., Acharya, B.S., Panda, A.K. Enhanced UV absorbance and photoluminescence properties of ultrasound assisted synthesized gold doped ZnO nanorods, (2014) Optical Materials, 36 (8), pp. 1402-1407.
11. J. Hyung, J. Yun, K. Cho, I. Hwang, J. Lee, S. Kim, Necked ZnO nanoparticle-based NO_2 sensors with high and fast response, Sens. Actuators B: Chem. 140 (2009) 412–417.
12. M.C. Carotta, A. Cervi, V. Natale, S. Gherardi, A. Giberti, V. Guidi, et al., ZnO gas sensors: a comparison between nanoparticles and nano tetrapods-based thick films, Sens. Actuators B: Chem. 137 (2009) 164–169.
13. P. Rai, Y.-S. Kim, H.-M. Song, M.-K. Song, Y.-T. Yu, The role of gold catalyst on the sensing behaviour of ZnO nanorods for CO and NO_2 gases, Sens. Actuators B: Chem. 165 (2012) 133–142.
14. P. Singh, V.N. Singh, K. Jain, T.D. Senguttuvan, Pulse-like highly selective gas sensors based on ZnO nanostructures synthesized by a chemical route: effect of in doping and Pd loading, Sens. Actuators B: Chem. 166–167 (2012) 678–684.
15. S.-J. Jung, H. Yanagida, The characterization of a CuO/ZnO hetero contact-type gas sensor having selectivity for CO gas, Sens. Actuators B: Chem. 37 (1996) 55–60.
16. J. Choi, G. Choi, Electrical and CO gas sensing properties of layered ZnO–CuO sensor, Sens. Actuators B: Chem. 69 (2000) 120–126.
17. C.S. Dandeneau, Y. Jeon, C.T. Shelton, T.K. Plant, D.P. Cann, B.J. Gibbons, Thin film chemical sensors based on p-CuO/n-ZnO hetero contacts, Thin Solid Films, 517 (2009), 4448–4454.

18. S. Ayg, D. Cann, Hydrogen sensitivity of doped CuO/ZnO hetero contact sensors, Sens. Actuators B: Chem. 106 (2005) 837–842.
19. X.H. Liu, J. Zhang, X.Z. Guo, S.H. Wu, S.R. Wang Amino acid-assisted one-pot assembly of Au, Pt nanoparticles onto one dimensional ZnO microrods. Nanoscale, 2 (2010), pp. 1178–1184.
20. Y. Zhang, Q. Xiang, J.Q. Xu, P.C. Xu, Q.Y. Pan, F. Li Self-assemblies of Pd nanoparticles on the surfaces of single crystal ZnO nanowires for chemical sensors with enhanced performances. Journal of Materials Chemistry, 19 (2009), pp. 4701–470.
21. A. Kolmakov, D.O. Klenov, Y. Lilach, S. Stemmer, M. Moskovits Enhanced gas sensing by individual SnO_2 nanowires and nanobelts functionalized with Pd catalyst particles. Nano Letters, 5 (2005), pp. 667–673.
22. Q. Xiang, G.F. Meng, H.B. Zhao, Y. Zhang, H. Li, W.J. Ma, J.Q. Xu Au nanoparticle modified WO_3 nanorods with their enhanced properties for photocatalysis and gas sensing. Journal of Physical Chemistry C, 114 (2010), pp. 2049–2055.
23. J. Zhang, X.H. Liu, X.Z. Guo, S.H. Wu, S.R. Wang A general approach to fabricate diverse noble-metal (Au, Pt, Ag, Pt/Au)/Fe_2O_3 hybrid nanomaterials. Chemistry- A European Journal, 16 (2010), pp. 8108–8116.
24. Jia, C., Zhong, W., Deng, M., Jiang, J. Microscopic Insight into the Activation of O2 by Au Nanoparticles on ZnO (101) Support, (2016) Journal of Physical Chemistry C, 120 (8), pp. 4322-4328.
25. Li, F., Zhang, L., Wu, S., Li, Z., Wang, Y., Liu, X. Au nanoparticles decorated ZnO nanoarrays with enhanced electron field emission and optical absorption properties, (2015) Materials Letters, 145, pp. 209-211.
26. Georgiev, P., Kaneva, N., Bojinova, A., Papazova, K., Mircheva, K., Balashev, K. Effect of gold nanoparticles on the photocatalytic efficiency of ZnO films (2014) Colloids and Surfaces A: Physicochemical and Engineering Aspects, 460, pp. 240-247.
27. Shinde S.D., Patil G.E., Kajale D.D., Gaikwad V.B., Jain G.H. Synthesis of ZnO nanorods by spray pyrolysis for H 2S gas sensor (2012) Journal of Alloys and Compounds, 528, pp. 109-114.
28. Yamazoe, N., Sakai, G., Shimanoe, K., Oxide semiconductor gas sensors, Catalysis Surveys from Asia, Vol. 7, Issue 1, (2003) pp. 63-75
29. C. Zhang, A. Boudiba, P. De Marco, et al. (2013), Room temperature responses of visible-light illuminated WO_3 sensors to NO_2 in the sub-ppm range. Sensors and Actuators B, 181, 395-401.
30. Ao, D., Ichimura, M. UV irradiation effects on hydrogen sensors based on SnO_2 thin films fabricated by the photochemical deposition, (2012) Solid-State Electronics, 69, pp. 1-3.
31. Park, S., An, S., Mun, Y., Lee, C. UV-enhanced NO_2 gas sensing properties of SnO 2-Core/ZnO-shell nanowires at room temperature, (2013) ACS Applied Materials and Interfaces, 5 (10), pp. 4285-4292.

32. A.J. Morfa, G. Beane, B. Mashford, B. Singh, E. Della Gaspera, A. Martucci, P. Mulvaney. Fabrication of ZnO Thin Films from Nanocrystal Inks J. Phys. Chem. C (2010) 114, 19815-19821.
33. Monakhov, E.V., Kuznetsov, A.Yu., Svensson, B.G. Zinc oxide: Bulk growth, role of hydrogen and Schottky diodes, (2009) Journal of Physics D: Applied Physics, 42 (15).
34. Wang, X.J., Vlasenko, L.S., Pearton, S.J., Chen, W.M., Buyanova, I.A. Oxygen and zinc vacancies in as-grown ZnO single crystals, (2009) Journal of Physics D: Applied Physics, 42 (17).
35. T. Seiyama, A. Kato, K. Fujiishi, M. Nagatani, A new detector for gaseous components using semiconductive thin films, Anal. Chem. 34 (1962) 1502–1503.
36. N. Koshizaki, T. Oyama, Sensing characteristics of ZnO-based NO_x sensor, Sens.Actuators B: Chem. 66 (2000) 119–121.
37. G.S. Trivikrama Rao, D. Tarakarama Rao, Gas sensitivity of ZnO based thick film sensor to NH_3 at room temperature, Sens. Actuators B: Chem. 55 (1999)166–169.
38. C. Zhang, M. Debliquy, H. Liao, Deposition and microstructure characterization of atmospheric plasma-sprayed ZnO coatings for NO_2 detection, Appl. Surf. Sci.256 (2010) 5905–5910.
39. S.-Y. Tsai, M.-H. Hon, Y.-M. Lu, Fabrication of transparent p-NiO/n-ZnO hetero-junction devices for ultraviolet photodetectors, Solid-State Electron. 63 (2011)37–41.
40. K. Hara, T. Horiguchi, T. Kinoshita, Highly efficient photon-to-electron conversion with mercurochrome-sensitized nano porous oxide semiconductor solar cells, Solar Energy Mater. Solar Cells 64 (2000) 115–134.
41. Bora, T., Myint, M.T.Z., Al-Harthi, S.H., Dutta, J. Role of surface defects on visible light enabled plasmonic photocatalysis in Au-ZnO nanocatalysts, (2015) RSC Advances, 5 (117), pp. 96670-96680.
42. Li, C., Lin, Y., Li, F., Zhu, L., Meng, F., Sun, D., Zhou, J., Ruan, S. Synthesis and highly enhanced acetylene sensing properties of Au nanoparticle decorated hexagonal ZnO nanorings (2015) RSC Advances, 5 (106), pp. 87132-87138
43. Mun, Y., Park, S., An, S., Lee, C., Kim, H.W. NO_2 gas sensing properties of Au-functionalized porous ZnO nanosheets enhanced by UV irradiation(2013) Ceramics International, 39 (8), pp. 8615-8622.
44. Gogurla, N., Sinha, A.K., Santra, S., Manna, S., Ray, S.K. Multifunctional Au-ZnO plasmonic nanostructures for enhanced UV photodetector and room temperature NO sensing devices (2014) Scientific Reports, 4, art. no. 6483.
45. B. Fabbri, A. Gaiardo, A. Giberti, V. Guidi, C. Malagù, A. Martucci, M. Sturaro G. Zonta, S. Gherardi, P.Bernardoni, Chemoresistive properties of photo-activated thin and thick ZnO films, Sensors and actuators B (2016), Vol. 222, pp. 1251–1256.
46. A. Giberti, B. Fabbri, A. Gaiardo, V. Guidi, C. Malagù, Resonant photoactivation of cadmium sulfide and its effect on the surface chemical activity, Applied Physics Letters 104, (2014), 222102.

47. J.D. Prades et al. (2009): Equivalence between thermal and room temperature UV light-modulated responses of gas sensors based on individual SnO_2 nanowires. Sensors and Actuators B, 140, 337-341.
48. A. Martucci, M. Pasquale, M. Guglielmi, M. Post, J.C. Pivin, Nanostructured silicon oxide nickel oxide sol-gel films with enhanced optical carbon monoxide gas sensitivity J. Am. Ceram. Soc. 86, 1638 (2003).
49. NIOSH Pocket Guide to Chemical Hazards, 2004 published by the National Institute for Occupational Safety and Health (NIOSH).
50. Threshold Limit Values & Biological Exposure Indices, copyright 2005 by the American Conference of Governmental Industrial Hygienists (ACGIH).
51. Gaiardo, A., Fabbri, B., Guidi, V., Bellutti, P., Giberti, A., Gherardi, S., Vanzetti, L., Malagù, C., Zonta, G. Metal sulfides as sensing materials for chemoresistive gas sensors, (2016) Sensors (Switzerland), 16 (3).
52. S. Sakka, H. Kozuka, Sol-gel preparation of coating films containing noble metal colloids. J. Sol–Gel Sci. Technol. 13, 701 (1998).
53. B.F.G. Johnson, R. Davis, in: J.C. Bailer Jr., H.J. Emeleus, R.Nyholm, A.F. Trotman-Dickenzon, "Comprehensive Inorganic Chemistry", vol. 3, (Pergamon, New York, 1973) p. 129.
54. Rishi Vyas, Sarla Sharma, Parul Gupta, Arun K. Prasad, S.K. Dhara, A.K. Tyagi, K. Sachdev, S.K. Sharma, Nitrogen dioxide induced conductivity switching in ZnO thin film Journal of Alloys and Compounds 571 (2013) 6–11.
55. C.Malagù, M.C. Carotta, S. Galliera, V. Guidi, T.G.G. Maffeis, G. Martinelli, G.T. Owen, S.P. Wilks, Evidence of bandbending flattening in 10 nm polycrystalline SnO_2, Sensors and Actuators B, 103/1-2 (2004) 50-54.
56. Hao Chen, Yuan Liu, Changsheng Xie, Jun Wu, Dawen Zeng, Yichuan Liao, A comparative study on UV light activated porous TiO_2 and ZnO film sensors for gas sensing at room temperature, Ceramics International, Volume 38, Issue 1, January 2012, Pages 503-509.
57. Alenezi M.R., Alshammari A.S., Jayawardena K.D.G.I., Beliatis M.J., Henley S.J., Silva S.R.P. Role of the exposed polar facets in the performance of thermally and UV activated ZnO nanostructured gas sensors (2013) Journal of Physical Chemistry C, 117 (34), pp. 17850-17858.
58. P.K. Chen, G.J. Lee, S.H. Davies, S.J. Masten, R. Amutha, J.J. Wu, Hydrothermal synthesis of coral-like Au/ZnO catalyst and photocatalytic degradation of OrangeII dye, Mater. Res. Bull. 48 (2013), pp. 2375–2382.
59. V. Iliev, D. Tomova, L. Bilyarska, A. Eliyas, Influence of the size of gold nanoparticles deposited on TiO_2 upon the photocatalytic destruction of oxalic acid, J. Mol. Catal. A: Chem. 263 (2007), pp. 32–38.
60. S. Matsushima, Y. Teraoka, N. Miura, N. Yamazoe, Electronic interaction between metal additives and tin dioxide in tin dioxide-based gas sensors, Jpn. J. Appl. Phys. 27 (1988), pp. 1798–1802.

61. T.A. Baker, X. Liua, C.M. Friend, The mystery of gold's chemical activity: local bonding, morphology and reactivity of atomic oxygen, Phys. Chem. Chem. Phys. 13 (2011), pp. 34–46.
62. Maxwell, I., Driving forces for innovation in applied catalysis, Stud. Surf. Sci. Catal. (1996) 101, pp. 1-9.
63. Wickham, D. T., Parker, D. H., Kastanas, G. N., Lazaga, M. A., Koel, B. E. , Reactivity of oxygen ad atoms on the Au (111) surface, Prepr. – Am. Chem. Soc., Div. Pet. Chem. (1992) 37, pp. 1034-1037.
64. Haruta, M., Tsubota, S., Kobayashi, T., Kageyama, H., Genet, M.J., Delmon, B. Low-Temperature Oxidation of CO over Gold Supported on TiO_2, α-Fe_2O_3, and Co_3O_4, J. Catal. (1993) 144, pp. 175-192.
65. Sarina, S., Waclawik, E.R., Zhu, H. Photocatalysis on supported gold and silver nanoparticles under ultraviolet and visible light irradiation (2013) Green Chemistry, 15 (7), pp. 1814-1833.
66. Mukherjee, S., Libisch, F., Large, N., Neumann, O., Brown, L.V., Cheng, J., Lasiter, J.B., Carter, E.A., Nordlander, P., Halas, N.J. Hot electrons do the impossible: Plasmon-induced dissociation of H_2 on Au, (2013) Nano Letters, 13 (1), pp. 240-247.